

## Article

# Numerical Study on Thermal Management of Air-Cooling Model for Diamond, Triangular and Rectangular Lithium-Ion Batteries of Electric Vehicles

Yun Gao \*, Wujun Ji and Xiaoqiang Chen

College of Automotive Engineering, Henan Polytechnic, Zhengzhou 450046, China; jwj2005326@126.com (W.J.); 37070@hnzj.edu.cn (X.C.)

\* Correspondence: gyauto@hnzj.edu.cn

**Abstract:** To improve the safety of electric vehicles, this paper analyzes the way of cooling lithium-ion batteries of electric vehicles and proposes an air-cooling scheme. First, a heat-generation model for the lithium-ion battery is prepared for numerical simulation and a finned air-cooling model is designed, which combines cold air with fins to lower the temperature of lithium-ion batteries. Through feasibility analysis, it is proved that the heat-generation model can reflect the actual heat generation of lithium-ion batteries. The cooling effect of the finned air-cooling model is also evaluated. The temperature can be 23.6 °C lower than the maximum compared with lithium-ion batteries without cooling. The cooling effect is desirable for diamond, triangle and rectangular lithium-ion battery packs, among which the rectangular battery pack achieves the most desirable effect. To conclude, to ensure the safe operation of lithium-ion batteries in electric vehicles, air cooling can be used to control their temperature, with the cooling effect in the rectangular lithium-ion battery pack being the most desirable.



**Citation:** Gao, Y.; Ji, W.; Chen, X. Numerical Study on Thermal Management of Air-Cooling Model for Diamond, Triangular and Rectangular Lithium-Ion Batteries of Electric Vehicles. *Processes* **2022**, *10*, 1104. <https://doi.org/10.3390/pr10061104>

Academic Editors: Manh-Kien Tran and Michael Fowler

Received: 24 April 2022

Accepted: 31 May 2022

Published: 1 June 2022

**Publisher's Note:** MDPI stays neutral with regard to jurisdictional claims in published maps and institutional affiliations.



**Copyright:** © 2022 by the authors. Licensee MDPI, Basel, Switzerland. This article is an open access article distributed under the terms and conditions of the Creative Commons Attribution (CC BY) license (<https://creativecommons.org/licenses/by/4.0/>).

**Keywords:** electric vehicle; lithium-ion battery; air cooling; thermal management

## 1. Introduction

Thanks to electric vehicles, environmental pollution has been greatly reduced and clean energy is put to good use. The battery pack, which powers electric vehicles, has attracted much attention with considerable research carried out to improve its performance. Currently, most electric vehicles run on lithium-ion batteries, which have the advantages of high voltage, large actual specific energy and long service life. However, high temperature produced from battery charging remains a problem that somehow affects the service life of the vehicle [1,2]. Therefore, it is necessary to apply thermal management to lithium-ion batteries, so that electric vehicles can be more efficient. Air cooling, as a way of cooling with low cost and good effect, is gaining more popularity among electric vehicle manufacturers. Existing studies on lithium-ion batteries have concluded that the battery cooling effect hinges on the shape of the battery pack [3–6]. Therefore, to improve the safety of lithium-ion batteries, this paper proposes an air-cooling model, and conducts numerical simulation on thermal management to explore the cooling effect of the finned air-cooling model on diamond, triangle and rectangular lithium-ion batteries, so as to promote the development of electric vehicles in China.

## 2. Literature Review

With more and more achievements made in the field of new energy, new energy products have caused a sensation. As a product of new energy development, electric vehicles are of great significance to social development. Therefore, there is no dearth of studies on electric vehicles. Polat et al. [7] used a Monte Carlo simulation to model the uncertain behavior of drivers and analyzed the impact of voltage drop, transformer load,

power loss and voltage imbalance on the low-voltage side of the distribution network. Results showed that when the popularity of electric vehicles reached 50%, there was a 25% probability of voltage violation [7]. To address the increasingly severe charging problem of electric vehicles, Kim and others put forward the charging demand prediction model of electric vehicles based on the Monte Carlo simulation, and used it to determine the peak load time of charging. The prediction model was proved effective [8]. To effectively stop the noise arising from electromagnetic interference when electric vehicles were traveling, scholars such as Chen proposed an estimation model for the electromagnetic interference of a resolver. The model was proved correct through simulation and actual measurement analysis, playing a significant role in analyzing the electromagnetic interference noise coupling between the motor drive system and other low pressure-sensitive circuits [9]. To address the charging management of electric vehicles, Qian and others put forward the necessity of effective management of the charging records of electric vehicles. They further proposed a distributed algorithm based on auction to calculate the optimal storage selection, and used the annealing algorithm to determine the server node allocation of each BC [10]. The effectiveness of the algorithm was verified. Ashfaq et al. [11] conducted research to evaluate the impact of electric vehicle development on social progress. They looked at the status quo and the development trend of electric vehicles in recent years, and analyzed the burden brought by electric vehicles on the power grid, providing theoretical reference for other studies on the same topic. Burkhart et al. [12] designed a one-mile electric vehicle to meet individual needs for transportation, and digitalized the process, thus reducing the complexity of the product and the manufacturing cost.

The battery is a key part of the energy vehicle. At present, most electric vehicles use lithium batteries. Falehi et al. [13] used the fractional hyper twist sliding mode control to improve the robustness of the battery storage system. Results show that the overshoot, undershoot and stability time of the system were 0.6, 0.4 and 0.03, respectively, indicating that the system had strong stability. To solve the problem of interface resistance between electrode and electrolyte of all solid-state lithium-ion batteries, Nishio and others [14] proposed to use “single-phase all solid-state batteries”. Results showed that the electronic leakage of the battery was significantly reduced. In addition, the battery had high lithium-ion conductivity with improved working voltage and reversible capacity. To cope with global warming and improve the performance of electric vehicles, Feng and others analyzed the heat dissipation effect of lithium-ion batteries of electric vehicles at different air inlet speeds, with different numbers of heat sinks and at different thicknesses of heat sinks between lithium batteries. They proposed an optimal scheme that could effectively improve the heat dissipation performance of lithium batteries, improve the performance of electric vehicles and reduce CO<sub>2</sub> emissions [15]. Wang and other scholars proposed a new mathematical evaluation method of power status to ensure the safety of the lithium battery pack [16]. By studying the non-convex optimization treatment of the lithium battery pack under complex working conditions, a complex evaluation model for evaluating the power status with coupling relationship decomposition was put in place. It was proved to effectively evaluate the power status on an on-going basis and was suitable for complex battery packs under complicated environments. Zhang et al. proposed an energy-management system based on a bus frequency signal to absorb as much photovoltaic output power as possible when the lithium battery was under fast-charging [17], whose effectiveness was verified through simulation experiments. To adjust the temperature of the graphite matrix in a passive way, Bang et al. [18] proposed a feasible solution to increase the temperature of the graphite matrix through the analysis of this finite element.

To sum up, the emergence of new energy has driven the rapid development of electric vehicles, resulting in increasing studies on this topic. To promote the sustainable development of electric vehicles, studies on lithium batteries have gone further. However, there are few studies on lithium batteries of electric vehicles, let alone studies on the cooling system of such batteries. Therefore, the air-cooling thermal management system for differ-

ent shapes of lithium batteries is analyzed in this paper through numerical simulation to provide theoretical support for the development of electric vehicles.

### 3. The Simulated Air-Cooling System for Lithium-Ion Batteries of Electric Vehicles

#### 3.1. Heat Generation Model for the Lithium-Ion Battery

To fully understand the working condition of the thermal management system when the lithium-ion battery is being cooled, this study first tries to understand how the battery generates heat and, based on the battery thermoelectric coupling model, it analyzes the heat generation and heat transfer phenomenon during the battery charging process [18–23]. During such a process, most electric energy is converted into chemical energy while some is converted into thermal energy, and the electric heating capacity of the battery will keep part of the generated heat inside the battery [24–26]. Equation (1) refers to the heat generation power of battery coil core.

$$\dot{Q} = \dot{Q}_j + \dot{Q}_r = I(U_o - U_t) + IT_0 \frac{\partial U_o}{\partial T} \quad (1)$$

In Equation (1),  $\dot{Q}$  represents the Joule thermal power of the battery and  $\dot{Q}_r$  represents the thermal power generated by the chemical reaction during energy conversion in the battery, the unit of which is W;  $I$  represents the current generated during battery charging, the unit of which is A;  $U_o$  represents the open circuit voltage of the battery;  $U_t$  represents the voltage at both ends of the positive and negative poles of the battery, the unit of which is; and  $T_0$  represents the ambient temperature,  $T$  representing the internal temperature of the battery, the unit of which is °C. The lithium-ion battery of electric vehicles contains a large number of modules where the contact resistance will be generated when the pole lug is connected with the bus bar. When the current is transmitted in the pole lug, the contact surface will shrink, which will produce resistance [27,28]. With the change of the roughness of the contact surface and the increase of the resistance, electric energy will be converted to thermal energy. The analysis of the contact resistance between the two is shown in Equation (2).

$$R_c = \frac{k}{0.102F} \quad (2)$$

In Equation (2),  $k$  represents the resistance coefficient, which is related to the surface properties of the contact material, and  $F$  represents the foundation pressure generated at the contact point. After the contact resistance is calculated, the energy variation caused by the current passing through the basic resistance is calculated according to Joule's law, as shown in Equation (3).

$$\dot{Q}_t = I^2 R_c \quad (3)$$

In Equation (3),  $I$  represents the passing current and  $R_c$  represents the contact resistance value. In the process of the battery charging, the heat generated will be transferred. In the study, only the heat conduction in the process of battery charging is taken into account, as shown in Equation (4).

$$\rho C_p \frac{\partial T}{\partial t} = \frac{\partial}{\partial x} (\lambda_x \frac{\partial T}{\partial x}) + \frac{\partial}{\partial y} (\lambda_y \frac{\partial T}{\partial y}) + \frac{\partial}{\partial z} (\lambda_z \frac{\partial T}{\partial z}) + \dot{Q} \quad (4)$$

In Equation (4),  $\rho$  represents the density of the battery coil,  $C_p$  represents the specific heat capacity of the battery coil,  $\lambda_x$  represents the thermal conductivity of the battery in direction X,  $\lambda_y$  represents the thermal conductivity of the battery in direction Y,  $\lambda_z$  represents the thermal conductivity of the battery in direction Z,  $\dot{Q}$  represents the thermal power of the battery, and  $T$  represents the internal temperature of the battery.

The heat-generation model for the lithium-ion battery is built to reflect the energy variation of the battery in the charging process, but the contact area between the environment and the battery will affect the effect of heat generation. Therefore, this paper designs

a method that can fully reflect the heat-generation effect of the lithium-ion battery in the charging process, as shown in Figure 1.

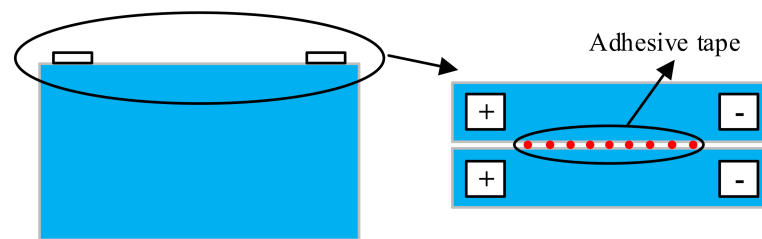


**Figure 1.** Schematic diagram of the heat-generation model for the lithium-ion battery.

Figure 1 shows that in the heat-generation test, two new batteries are selected to ensure that they can produce the same heat in the charging process. At the same time, they are wrapped with insulating cotton to reduce heat loss. The location of the thermocouple is determined, the wrapped batteries are connected to the charging and discharging motor and the thermocouple data collector is used to collect data.

### 3.2. The Air-Cooling Model for Lithium-Ion Battery

To address the heat generated by the lithium-ion battery in the charging process, most of existing studies proposed to build a battery pack thermal management system based on water cooling, but the water-cooling device is complicated and expensive [29–33]. To reduce the complexity and manufacturing cost, an air-cooling model is proposed. At the same time, to reduce energy consumption caused by high ambient temperature, a finned heat-exchange equipment is imbedded in the air-cooling thermal management system, as shown in Figure 2.

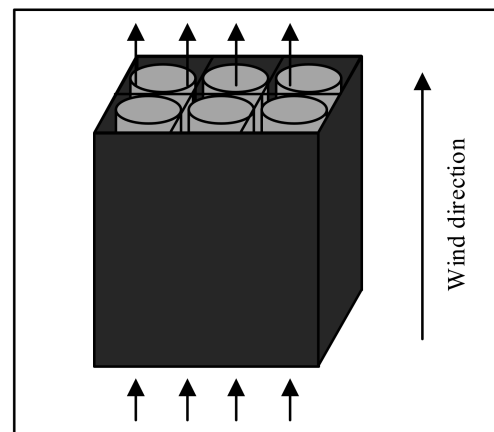


**Figure 2.** Finned air-cooling thermal management system.

Figure 2 shows that since the lithium-ion battery pack is composed of multiple single batteries in series and in parallel; when analyzing the system structure, the edge of the battery module can be ignored and considered as multiple repeating units. Therefore, the simulation unit is used in the numerical simulation to reduce calculation. In the finned air-cooling model, the fin is placed in the battery gap, as high as the battery. The cold air flows between the fin and the battery. The cold air is used for heat exchange and takes away the heat generated during the charging process. To simplify the numerical calculation, it is assumed that the physical properties of the battery do not change with the environment. It is also assumed that the heat-generation rate is the same everywhere in the battery. In addition, heat radiation generated on the battery surface is ignored. Finally, the flow of cold air in the gap is regarded as incompressible. The governing equations and boundary conditions in numerical simulation are determined. First, the energy equation of

the battery area is defined as Equation (4). Second, the energy-control equation inside the fin is determined. Since the heat accumulation inside the fin is caused by heat conduction, the energy-control equation can be defined as Equation (5).

$$\rho_f C_{p,f} \frac{\partial T_f}{\partial t} = \lambda_f \frac{\partial T_f}{\partial x} + \lambda_f \frac{\partial T_f}{\partial y} + \lambda_f \frac{\partial T_f}{\partial z} \quad (5)$$

In Equation (5),  $\rho_f$  represents the density of the fin,  $C_{p,f}$  represents the specific heat capacity of the fin,  $\lambda_f$  represents the thermal conductivity of the fin and  $T_f$  represents the temperature of the fin in numerical simulation. Finally, the internal energy of the cold air is determined and its energy source is the heat conduction and heat convection between the battery and the fin. Therefore, its energy control equation can be defined as Equation (6).

$$\rho_a C_{p,a} \frac{\partial T_a}{\partial t} = \nabla(\lambda_a \nabla T_a) + \rho_a C_{p,a} u_a \nabla T_a \quad (6)$$

In Equation (6),  $u_a$  represents the air flow rate. The incompressible air flow equation is shown in Equation (7).

$$\rho_a \frac{\partial u_a}{\partial t} = \rho_a g_a - \nabla p_a + u_a \nabla^2 u_a \quad (7)$$

In Equation (7),  $g_a$  represents gravitational acceleration and  $p_a$  represents air pressure.

In the boundary condition control, the initial conditions are determined, as shown in Equation (8).

$$\begin{cases} T_a = T_f = T_0 \\ u_a = \text{constant} \end{cases} \quad (8)$$

In Equation (8),  $T_f$  represents the initial temperature of the fin,  $T_a$  represents the initial temperature of the air,  $T_0$  represents the ambient temperature and the reduction is defined as 25 °C;  $u_a$  indicates the initial air velocity. The temperature boundary conditions are also defined, as shown in Equation (9).

$$\begin{cases} \lambda_b \nabla T_b = \lambda_f \nabla T_f \\ \lambda_b \nabla T_b = \lambda_a \nabla T_a \end{cases} \quad (9)$$

Equation (9) shows that the energy of the inflow interface and that of the outflow interface on the contact surface between the battery and the fin. The battery and the air are equal.  $\lambda_b$  represents the thermal conductivity of the battery and  $T_b$  represents the temperature of the battery;  $\lambda_f$  represents the thermal conductivity of the fin and  $T_f$  represents the temperature of the fin;  $\lambda_a$  represents the thermal conductivity of air and  $T_a$  represents the air temperature. In the lithium-ion battery pack, the upper and lower surfaces will be equipped with circuit boards, which can be regarded as thermal insulation, which means no energy in this area. Finally, the velocity boundary condition is defined, and the inlet and outlet boundary condition of air is defined as Equation (10).

$$\begin{cases} u_{a,in} = \text{constant} \\ p_a = p_0 = 101.325 \text{ KPa} \end{cases} \quad (10)$$

In Equation (10),  $u_{a,in}$  represents the constant velocity of the air at the inlet and  $p_a$  represents the pressure at the outlet, which is positioned at the standard atmospheric pressure. It is believed that air is a Newtonian fluid, which means when air flows in the gap between the battery and the fin, the velocity is 0. In numerical simulation, the finite element solution is adopted, the process of which is shown in Figure 3.

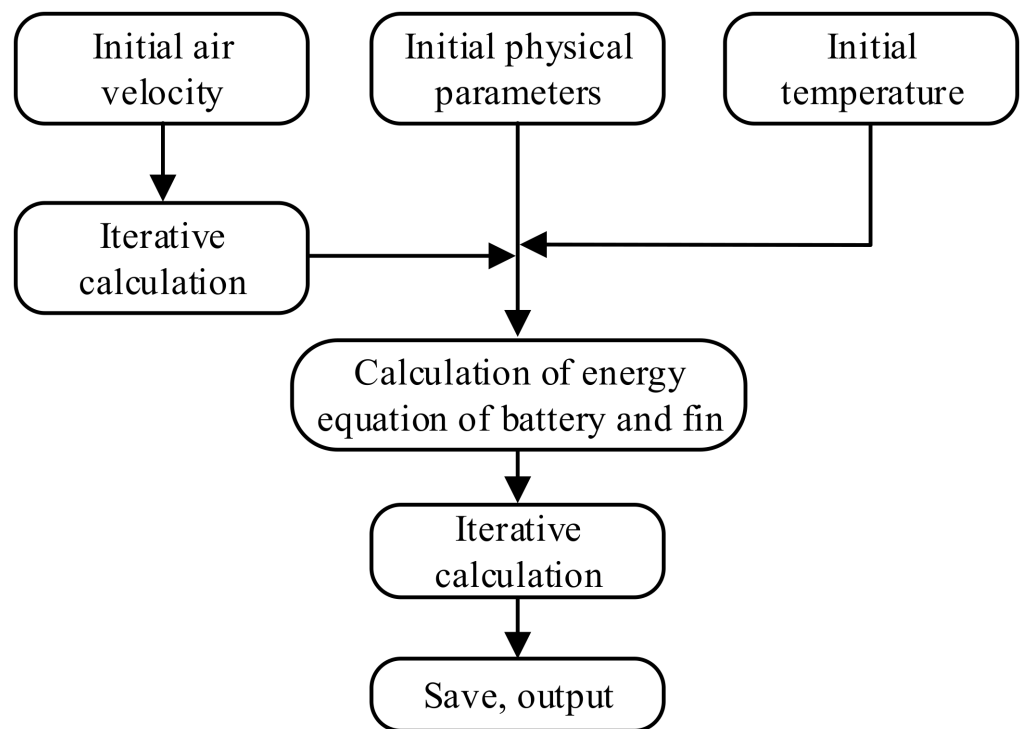


**Figure 3.** Flow chart of numerical simulation.

Figure 3 shows that with the support of finite element technology, the physical characteristics and boundary conditions of the lithium-ion battery pack are first input as the initial values, which are iteratively calculated through the air-flow equation. With the output of the distribution of air velocity field, the energy equation of the battery and the fin is calculated according to the set time and the initial temperature. The temperature distribution in the simulation unit is obtained by continuous iterative solution.

#### 4. Numerical Simulation on the Air-Cooling Model for the Lithium-Ion Battery Pack

##### 4.1. Demonstration for the Simulated Heat Generation Effect of the Heat-Generation Model

Numerical simulation is an approach to simulate the system environment on the computer, so as to determine the scientificity and feasibility of the algorithm or model. In addition, numerical simulation can help researchers find the optimal parameters of the model, so as to optimize the model and achieve the best performance in practical application. The heat-generation model is the key part in the numerical analysis of the air-cooling thermal management system for the lithium-ion batteries of electric vehicles. Therefore, this paper creates a simulated environment to analyze the performance of the heat-generation model.

It can be seen from Figure 4 that by analyzing the temperatures of the three monitoring points, the heat-generation model is proved to be effective. At monitoring point 1, the temperature generated in the simulated environment increases along with the charging time, and it reaches the highest temperature, 35.7 °C, at 4000 s. The maximum deviation from the actual temperature is only 1.3%. At monitoring point 0 and monitoring point 3, the deviation between the simulated temperature and the actual temperature is within 1.2%. The above results show that the simulated heat-generation model for the lithium-ion battery is consistent with the actual heat. A monitoring point is studied as a case to analyze the temperature variation of the heat-generation model under different magnification, as shown in Figure 5.

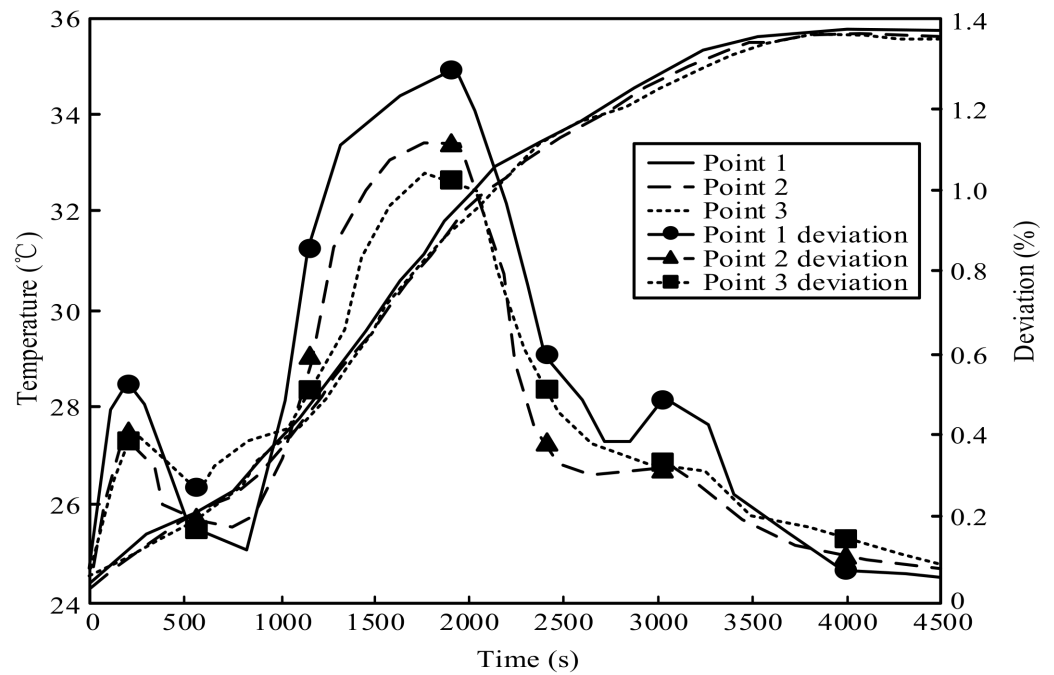


**Figure 4.** Analysis of the performance of the heat-generation model.

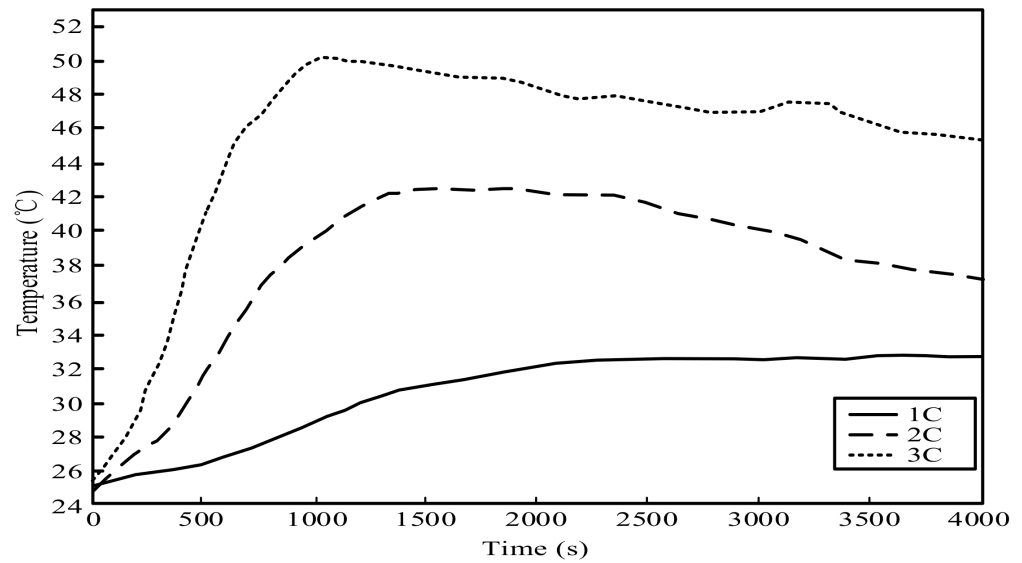


**Figure 5.** Temperature variation of heat-generation model under different magnification.

It can be seen from Figure 5 that at the current monitoring point, with the prolonging of the charging time, the temperature rises at a different rate and the maximum temperature varies under different magnification. At the charging rate of 1C, when charging for 2800 s, the temperature of the current monitoring point is neither high nor low, and it reaches the maximum of 32.7 °C at 3600 s. At the charging rate of 2C, the temperature of the current monitoring point is stable when charged for 1700 s. When charged for 1800 s, the temperature reaches the maximum, which is 42.5 °C. After that, the temperature begins to decrease. At the charging rate of 3C, the charging time required for the current monitoring point to reach the highest temperature is shortened to 1200 s, with the highest temperature being 50.1 °C. In addition, this paper also analyzes the simulated temperature distribution of the lithium-ion battery pack, as shown in Figure 6.

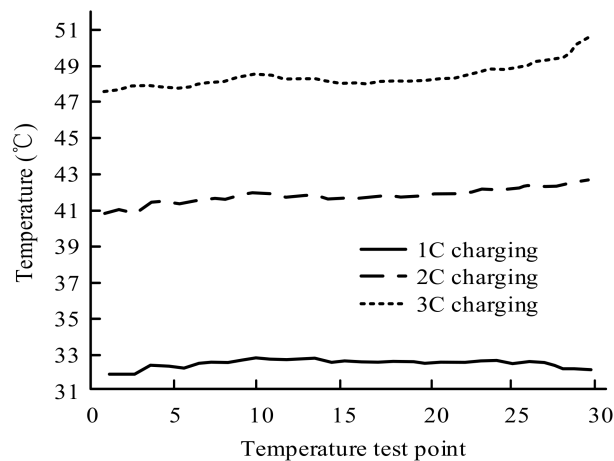


**Figure 6.** Simulated temperature distribution of lithium-ion battery pack.

From the comprehensive analysis of 30 monitoring points in the battery pack as shown in Figure 6, it is found that at the charging rate of 1C, the highest temperature of the battery pack is 32.9 °C, whereas the lowest is 31.8 °C, with a gap of 1.1 °C. At the charging rate 2C, the temperature of the battery pack rises significantly to 42.6 °C to the maximum, and the bottom line is 40.8 °C. At the charging rate of 3C, the temperature of the battery pack rises to 50.4 °C to the maximum. From the temperature distribution of the battery pack in the heat generation model, there is a huge temperature gap at different monitoring points, which means that during the charging process, the contact resistance between the contact points in the lithium-ion battery pack are constantly changing, resulting in insufficient current carrying in some monitoring point areas with the increase of the magnification.

#### 4.2. Numerical Simulation Analysis of the Finned Air-Cooling Effect

The main purpose of finned air-cooling is to reduce the heat generated by lithium-ion batteries during the charging process. To understand the cooling effect of the finned air-cooling model, this paper applies numerical simulation to the heat-generation model, and analyzes how the temperature is lowered under finned air-cooling and water-cooling conditions, respectively, as shown in Figure 7.

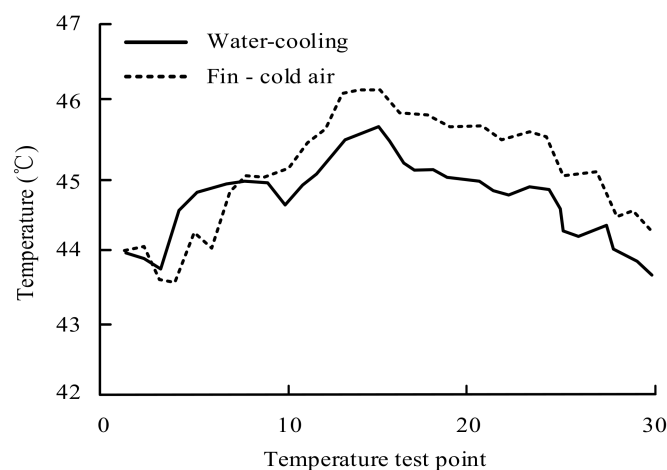


**Figure 7.** Comparison of the cooling effect under finned air-cooling and water-cooling conditions.

As can be seen from Figure 7, the simulation is conducted at the charging rate of 3C, with obvious temperature rise. The temperature at 30 monitoring points in the battery pack is detected. Under the water-cooling condition, the overall temperature of the battery pack is neither too high nor too low, which is around 45 °C, shifting between 43.7 °C and 45.9 °C. Under the finned air-cooling condition, the highest temperature of the lithium-ion battery

pack is 46.1 °C while the lowest is 43.6 °C. From the comparison of the two conditions, it can be found that water cooling achieves a better effect in lowering the temperature. The reason is that water can take away the heat of the battery through its flow, so that the battery can be wrapped in a relatively low-temperature environment for a long time. However, at the same charging rate, both ways can effectively control the battery pack temperature and, if the cost is considered, the finned air-cooling model is better than the water-cooling one, which further proves the availability and performance of the cooling model proposed in this study. In addition, this paper further probes into the cooling effect of the finned air-cooling model on reducing the temperature of the battery pack at different charging rates, as shown in Figure 8.

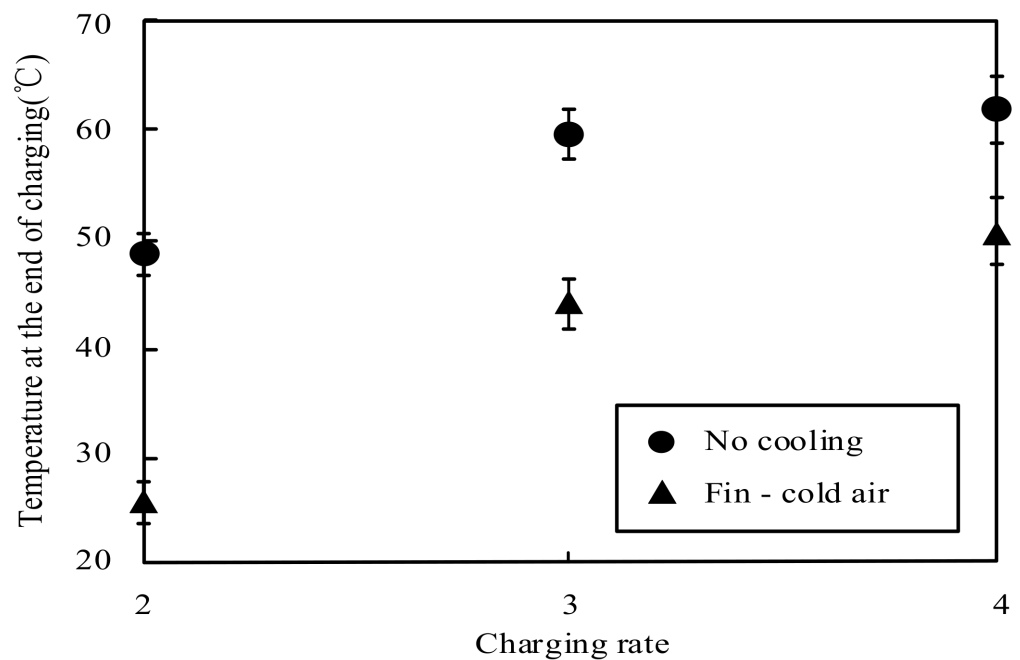


**Figure 8.** Finned air-cooling effect at different charging rates.

Figure 8 shows the final temperature of the lithium-ion battery pack with and without finned air-cooling. It can be found that at all charging rates, the final temperature of the lithium-ion battery pack without cooling is on the rise continuously. At the charging rate of 3C, the temperature can reach 63.4 °C, and at 1C, it can still climb to as high as 49.9 °C. When finned air-cooling is applied, the temperature of the lithium-ion battery pack at the charging rate of 3C is 51.1 °C, which is 12.3 °C lower than that without cooling. At the charging rate of 1C, the temperature is only 26.3 °C, 23.6 °C lower than that without cooling. The above results show that the finned air-cooling model can significantly reduce the heat generated in the charging process of the lithium-ion battery pack and ensure the service life of the battery.

#### 4.3. Numerical Analysis of Air-Cooling Thermal Management System with Different Battery Group Shapes

Finally, this paper studies the lithium-ion battery pack when it presents different shapes. There are three shapes: diamond, triangle and rectangle. The temperature variations of the battery pack with finned air-cooling in different shapes are analyzed. This paper analyzes the temperature in the convective heat-exchange area of the diamond, triangle and rectangle lithium-ion battery packs after the discharge is completed, as shown in Figure 9.

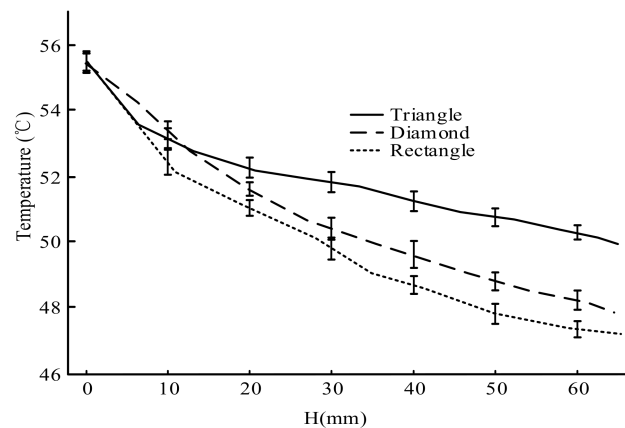


**Figure 9.** Temperature in the convective heat-exchange area of the diamond, triangle and rectangle lithium-ion battery packs when the discharging is completed.

As can be seen from Figure 9, the battery pack in different shapes has different temperatures in the same heat-exchange area. The temperature of a triangle battery pack is the highest, that of a rectangle pack is in the middle, while that of a diamond is the lowest. In addition, it can be seen from the temperature variation that when the discharging is finished, the temperature of the lithium-ion battery decreases with the increase of the heat-exchange area. The results show that the finned air-cooling method has a significant yet different cooling impact on the diamond, triangle and rectangle lithium-ion battery packs. Finally, numerical simulation is applied to measure the temperature of each monitoring point for three different shapes of battery packs with finned air-cooling, as shown in Figure 10.

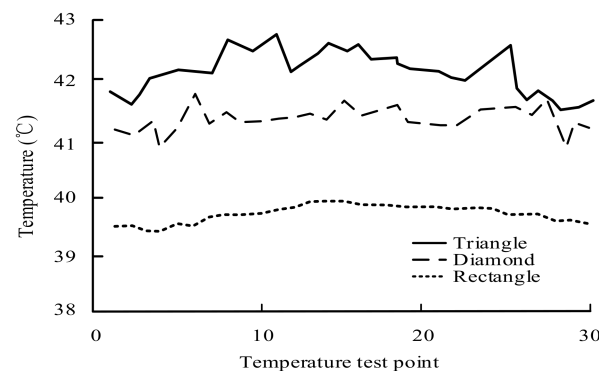


**Figure 10.** Numerical simulation on three different shapes of battery packs.

As can be seen from Figure 10, with finned air-cooling, the temperatures at each monitoring point for diamond, triangular and rectangular lithium-ion battery packs remain within a low range, in which the highest temperature is in the triangular battery pack, reaching 42.3 °C, and the lowest is in the rectangular battery pack, which is only 40.2 °C. At the same time, from the curve change, it can be found that the temperature at each monitoring point of a rectangular battery pack is relatively concentrated, while that of a triangular battery pack is relatively dispersed. To sum up, finned air-cooling can generate a good cooling effect on diamond, triangle and rectangle lithium-ion battery packs, and the rectangular battery pack has the most desirable cooling effect of the three. The reason is that in the rectangular battery pack, the finned air-cooling model generates the same influence on each battery, resulting in a more balanced cooling effect. The mutual influence between each battery is not strong. As a result, the overall cooling effect of the battery pack is optimal.

## 5. Conclusions

With the development of new energy sources, electric vehicles have gained popularity among people. As most electric vehicles run on lithium-ion batteries, to improve their service life, this paper puts forward an air-cooling model to lower the temperature in the lithium-ion battery pack. First, a heat-generation model of a lithium-ion battery is created for subsequent numerical simulation and a finned air-cooling method is designed to ensure the cooling effect of the lithium-ion battery. Results show that the heat-generation model can effectively reflect the temperature variation of lithium-ion batteries during the charging process. The finned air-cooling model has the same cooling effect as the water-cooling one, and the minimum temperature can be reduced to 43.6 °C. In addition, the maximum temperature difference between the pack with finned air-cooling and that without can be 23.6 °C. Finally, through the numerical simulation on diamond, triangle and rectangle lithium-ion battery packs with finned air-cooling, it is found that all three shapes of packs can achieve good cooling effects, among which the rectangular battery pack is the most desirable one. Therefore, it can be concluded that it is feasible to use air to cool the lithium-ion battery, and the rectangular lithium-ion battery pack has the most advantages in lowering the temperature.

**Author Contributions:** Conceptualization, Y.G.; data curation, X.C.; formal analysis, W.J.; investigation, W.J.; methodology, Y.G.; project administration, Y.G.; software, W.J.; validation, X.C.; writing—original draft, Y.G.; writing—review & editing, Y.G. All authors have read and agreed to the published version of the manuscript.

**Funding:** This study received no funding.

**Institutional Review Board Statement:** Not applicable.

**Informed Consent Statement:** Not applicable.

**Data Availability Statement:** The data presented in this study are available in the article.

**Conflicts of Interest:** The authors declare no conflict of interest.

## References

1. Lv, C.; Liu, Y.; Hu, X.; Guo, H.; Cao, D.; Wang, F.Y. Simultaneous observation of hybrid states for cyber-physical systems: A case study of electric vehicle powertrain. *IEEE Trans. Cybern.* **2018**, *48*, 2357–2367. [[PubMed](#)]
2. Chen, T.D.; Kockelman, K.M.; Khan, M. Locating electric vehicle charging stations: Parking-based assignment method for Seattle, Washington. *Transp. Res. Rec.* **2018**, *2385*, 28–36. [[CrossRef](#)]
3. Zhang, X.; Tang, Y.; Zhang, F.; Lee, C.S. A novel aluminum-graphite dual-ion battery. *Adv. Energy Mater.* **2016**, *6*, 1502588. [[CrossRef](#)]
4. Gong, D.; Wei, C.; Xie, D.; Tang, Y. Ultrasmall antimony nanodots embedded in carbon nanowires with three-dimensional porous structure for high-performance potassium dual-ion batteries. *Chem. Eng. J.* **2022**, *431*, 133444. [[CrossRef](#)]
5. Ji, B.; Zhang, F.; Song, X.; Tang, Y. A novel potassium-ion-based dual-ion battery. *Adv. Mater.* **2017**, *29*, 1700519. [[CrossRef](#)]
6. Sun, B.; Gao, S.; Ma, C.; Li, J. System power loss optimization of electric vehicle driven by front and rear induction motors. *Int. J. Automot. Technol.* **2018**, *19*, 121–134. [[CrossRef](#)]
7. Polat, Ö.; Eyüboğlu, O.H.; Gül, Ö. Monte Carlo simulation of electric vehicle loads respect to return home from work and impacts to the low voltage side of distribution network. *Electr. Eng.* **2021**, *103*, 439–445. [[CrossRef](#)]
8. Kim, C.Y.; Kim, C.R.; Cho, S.H. An analysis on the change of peak load time considering the forecasting of electric vehicle charging demand for apartment based on Monte Carlo simulation. *Trans. Korean Inst. Electr. Eng.* **2021**, *70*, 21–30. [[CrossRef](#)]
9. Chen, H.; Wang, T.; Ye, S.; Zhou, T. Modeling and suppression of electromagnetic interference noise on motor resolver of electric vehicle. *IEEE Trans. Electromagn. Compat.* **2021**, *63*, 720–729. [[CrossRef](#)]
10. Qian, L.P.; Wu, Y.; Xu, X.; Ji, B.; Shi, Z.; Jia, W. Distributed charging-record management for electric vehicle networks via blockchain. *IEEE Internet Things J.* **2021**, *8*, 2150–2162. [[CrossRef](#)]
11. Ashfaq, M.; Butt, O.; Selvaraj, J.; Rahim, N. Assessment of electric vehicle charging infrastructure and its impact on the electric grid: A review. *Int. J. Green Energy* **2021**, *18*, 657–686. [[CrossRef](#)]
12. Burkhart, J.; Breckle, T.; Merk, M.; Ramsaier, M.; Till, M.; Stetter, R. Customer-oriented digital design process for the development and production of an individual last-mile electric vehicle. *Procedia CIRP* **2021**, *100*, 542–547. [[CrossRef](#)]
13. Darvish Falehi, A.; Torkaman, H. Robust fractional-order super-twisting sliding mode control to accurately regulate lithium-battery/super-capacitor hybrid energy storage system. *Int. J. Energy Res.* **2021**, *45*, 18590–18612. [[CrossRef](#)]

14. Nishio, A.; Inoishi, A.; Kitajou, A.; Okada, S. Effect of Li<sub>3</sub>BO<sub>3</sub> addition to NASICON-type single-phase all-solid-state lithium battery based on Li<sub>1.5</sub>Cr<sub>0.5</sub>Ti<sub>1.5</sub>(PO<sub>4</sub>)<sub>3</sub>. *J. Ceram. Soc. Jpn.* **2019**, *127*, 18–21. [[CrossRef](#)]
15. Feng, X.; Hu, J. Analysis and optimization control of finned heat dissipation performance for automobile power lithium battery pack. *Therm. Sci.* **2020**, *24*, 132. [[CrossRef](#)]
16. Wang, S.L.; Stroe, D.I.; Fernandez, C.; Xiong, L.Y.; Fan, Y.C.; Cao, W. A novel power state evaluation method for the lithium battery packs based on the improved external measurable parameter coupling model. *J. Clean. Prod.* **2020**, *242*, 118506. [[CrossRef](#)]
17. Zhang, Y.; Wei, W. Model construction and energy management system of lithium battery, PV generator, hydrogen production unit and fuel cell in islanded AC microgrid. *Int. J. Hydrogen Energy* **2020**, *45*, 16381–16397. [[CrossRef](#)]
18. Tsao, B.; Chmiel, B.; Devillier, A.; Tsao, M.; McLeod, M.; Miller, K.; Schimpf, P.; Grigsby, A.; Fellner, J. Transient finite element simulation of a lithium-ion battery pack thermal management system based on latent heat system materials. *ECS Trans.* **2021**, *104*, 61–71. [[CrossRef](#)]
19. Wang, M.; Jiang, C.; Zhang, S.; Song, X.; Tang, Y.; Cheng, H.M. Reversible calcium alloying enables a practical room-temperature rechargeable calcium-ion battery with a high discharge voltage. *Nat. Chem.* **2018**, *10*, 667–672. [[CrossRef](#)]
20. Zhang, L.; Wang, X.; Zhang, Z.; Cui, Y.; Ling, L.; Cai, G. An adaptative control strategy for interfacing converter of hybrid microgrid based on improved virtual synchronous generator. *IET Renew. Power Gener.* **2022**, *16*, 261–273. [[CrossRef](#)]
21. Li, J.; Wang, F.; He, Y. Electric vehicle routing problem with battery swapping considering energy consumption and carbon emissions. *Sustainability* **2020**, *12*, 10537. [[CrossRef](#)]
22. Kang, W.; Zhao, Y.; Jia, X.; Hao, L.; Dang, L.; Wei, H. Paraffin/SiC as a novel composite phase-change material for a lithium-ion battery thermal management system. *Trans. Tianjin Univ.* **2021**, *27*, 55–63. [[CrossRef](#)]
23. Wang, Z.; Lei, Q.; Wang, Z.; Yuan, H.; Cao, L.; Qin, N.; Lu, Z.; Xiao, J.; Liu, J. In-situ synthesis of free-standing FeNi-oxyhydroxide nanosheets as a highly efficient electrocatalyst for water oxidation. *Chem. Eng. J.* **2020**, *395*, 125180. [[CrossRef](#)]
24. Du, J.; Mo, X.; Li, Y.; Zhang, Q.; Li, J.; Wu, X.; Lu, L.; Ouyang, M. Boundaries of high-power charging for long-range battery electric car from the heat generation perspective. *Energy* **2019**, *182*, 211–223. [[CrossRef](#)]
25. Saw, L.H.; Poon, H.M.; San Thiam, H.; Cai, Z.; Chong, W.T.; Pambudi, N.A.; King, Y.J. Novel thermal management system using mist cooling for lithium-ion battery packs. *Appl. Energy* **2018**, *223*, 146–158. [[CrossRef](#)]
26. Wang, X.; Xie, Y.; Day, R.; Wu, H.; Hu, Z.; Zhu, J.; Wen, D. Performance analysis of a novel thermal management system with composite phase change material for a lithium-ion battery pack. *Energy* **2018**, *156*, 154–168. [[CrossRef](#)]
27. Martin-Martin, L.; Gastelurrutia, J.; Larraona, G.S.; Anton, R.; del Portillo-Valdes, L.; Gil, I. Optimization of thermal management systems for vertical elevation applications powered by lithium-ion batteries. *Appl. Therm. Eng.* **2018**, *147*, 155–166. [[CrossRef](#)]
28. Chen, S.; Peng, X.; Bao, N.; Garg, A. A comprehensive analysis and optimization process for an integrated liquid cooling plate for a prismatic lithium-ion battery module—ScienceDirect. *Appl. Therm. Eng.* **2019**, *156*, 324–339. [[CrossRef](#)]
29. Wan, C. Battery space optimization to limit heat transfer in a lithium-ion battery using adaptive elephant herding optimization. *Ionics* **2020**, *26*, 4993–5009. [[CrossRef](#)]
30. Madani, S.S.; Schaltz, E.; Kær, S.K. Thermal analysis of an indirect liquid cooling with different geometries for a lithium-ion battery. *ECS Trans.* **2019**, *95*, 105–112. [[CrossRef](#)]
31. Wang, H.; Zheng, X.; Yuan, X.; Wu, X. Low-complexity model predictive control for a nine-phase open-end winding PMSM with dead-time compensation. *IEEE Trans. Power Electron.* **2022**, *37*, 8895–8908. [[CrossRef](#)]
32. Wang, H.; Wu, X.; Zheng, X.; Yuan, X. Virtual voltage vector based model predictive control for a nine-phase open-end winding PMSM with a common DC bus. *IEEE Trans. Ind. Electron.* **2022**, *69*, 5386–5397. [[CrossRef](#)]
33. Liu, F.F.; Lan, F.C.; Chen, J.Q.; Li, Y.G. Experimental investigation on cooling/heating characteristics of ultra-thin micro heat pipe for electric vehicle battery thermal management. *Chin. J. Mech. Eng.* **2018**, *31*, 179–188. [[CrossRef](#)]